Expert Systems with Applications 36 (2009) 7786–7797

Contents lists available at ScienceDirect

Expert Systems with Applications

journal homepage: www.elsevier.com/locate/eswa

Finding out general tendencies in speckle noise reduction in ultrasound images

Juan L. Mateo [a], Antonio Fernández-Caballero [a,b,*]

[a] Instituto de Investigación en Informática de Albacete (I3A), Universidad de Castilla-La Mancha, 02071 Albacete, Spain
[b] Departamento de Sistemas Informáticos, Universidad de Castilla-La Mancha, 02071 Albacete, Spain

ARTICLE INFO

Keywords:
Speckle noise
Digital image processing
Noise reduction
Ultrasound images

ABSTRACT

This article investigates and compiles some of the techniques mostly used in the smoothing or suppression of speckle noise in ultrasound images. With this information, a comparison of all the methods studied is done based on an experiment, using quality metrics to test their performance and show the benefits each one can contribute. To test the methods, a synthetic, noise-free image of a kidney is created and later simulations using Field II program to corrupt it are performed. This way, the smoothing techniques can be compared using numeric metrics, taking the noise-free image as a reference. Since real ultrasound images are already noise corrupted images and real noise-free images do not exist, conventional metrics cannot be used to indicate the quality obtained with filtering. Nevertheless, we propose the use of the tendencies observed in our study in real images.

1. Introduction

Medical images, such as magnetic resonance, X-rays, ultrasound, etc. are very useful tools for the diagnosis and study of various illnesses. Since the birth of Computer Science, this science has been a great help for Medicine in general and in particular in the medical image field. This paper focuses on ultrasound images and specifically on speckle noise suppression. Ultrasound images are degraded by an intrinsic artefact called "speckle", which is the result of the constructive and destructive coherent summation of ultrasound echoes.

Several techniques for suppressing speckle noise have been developed. According to the moment when the speckle reduction is produced, there are two basic approaches – the compounding approach and the post-processing approach (Adam, Beilin-Nissan, Friedman, & Behar, 2006). The compounding approach includes methods in which the data acquisition procedure has been modified to produce several images of the same region and combine them to form a single image (e.g. Behar, Adam, & Friedman, 2003; Jespersen, Wilhjelm, & Sillese, 1998; Stetson, Graham, & Macovski, 1997; Trahey, Smith, & Van Ramm, 1986). The post-processing approach includes many different filtering techniques that are implemented on the B-mode images after they have been generated. They are divided mainly into two classes: (i) techniques that are applied directly in the original image and (ii) techniques that are applied in the frequency domain (Stippel, Philips, & Lemahieu, 2002).

An example of compound approach Chen, Broschat, and Flynn (1996) proposes a hybrid phase-insensitive homomorphic processing technique for speckle reduction. Initially, several subimages are formed using separate portions of the transducer, then a log transform is applied to each subimage to destroy the phase relationship between the transducer element outputs. A low frequency emphasis filter is used to smooth high frequency components, and finally an exponential function is applied to recover the original signal level.

In recent years, much interest has been focused on the post-formation filtering methods applied directly in the original image methods. Approaches in this category include many fixed and adaptive filters, such as L_2-mean filter (Kotropoulos & Pitas, 1992), adaptive filter reduction (ASR) (Bernstein, 1987; Bamber & Daft, 1986), adaptive weighted median filter (AWMF) (Karaman, Kutay, & Bozdagi, 1995; Loupas, McDicken, & Allan, 1989), nonlinear diffusion (Abd-Elmoniem, Youssef, & Kadah, 2002; Yu & Acton, 2002), MAP estimation (Sanches & Marques, 2003) and so on.

Adaptive filtering algorithms continue being popular for speckle reduction. Chen, Yin, Flynn, and Broschat (2003) select a filtering region size using an appropriately estimated homogeneity value for region growth. Homogeneous regions are processed with an arithmetic mean filter. Edge pixels are filtered using a nonlinear median filter. More recently, to reduce the blurring in conventional distance-weighted (DW) interpolation, Huang, Zheng, Lu, and Chi (2005) proposed an improved method named as square–distance–weighted (SDW) interpolation, which used the square of the inverse distance as the weight for each pixel. And in Huang and Zheng (2006), a new adaptive algorithm based

* Corresponding author. Address: Departamento de Sistemas Informáticos, Universidad de Castilla-La Mancha, 02071 Albacete, Spain. Tel.: +34 967599200; fax: +34 967 599224.
E-mail addresses: jlmateo@dsi.uclm.es (J.L. Mateo), caballer@dsi.uclm.es (A. Fernández-Caballero).

0957-4174/$ - see front matter © 2008 Elsevier Ltd. All rights reserved.
doi:10.1016/j.eswa.2008.11.029

on SDW interpolation for volume reconstruction of 3D freehand ultrasound is introduced. Xiao, Su, and Chen (2004) present a diffusion stick method for speckle suppression in ultrasonic images. An asymmetric stick filter kernel is firstly defined by decomposing the rectangle neighbourhood into line segments of variable orientations. Then, the weighted sum of averages along each stick is used to produce the filtered images.

In the wavelet domain, recently, Thakur and Anand (2005) introduced the comparative study of various wavelet filter based denoising methods according to different thresholding values applied to ultrasound images. More works on wavelet domain thresholding may be found in Hao, Gao, and Gao (1999), Rakotomamonjy, Deforge, and Marche (2000), Zong, Laine, and Geisse (1998), among others. Also, a soft-threshold denoising method is presented by Donoho (1995), where the observed signal is decomposed into the wavelet domain.

One of the main problems when employing an image processing technique – looking for speckle reduction, in this case – is assessing its performance. The quality of a reconstructed image could be measured by the traditional distortion measures such as mean-square error (MSE), peak signal-to-noise ratio (PSNR), and correlation coefficients between the original and reconstructed images (Tolba, 2002). Adam et al. (2006) evaluate the effectiveness of speckle reduction in the ultrasound images for each simulated image, by statistically estimating three image quality parameters – contrast-to-noise ratio (CNR), lesion signal-to-noise ratio (LSNR) and signal-to-noise ratio (SNR), as defined in Chen et al. (1996). The parameter SNR is used to evaluate the improvements in smoothing, as observed in homogeneous regions of an image (speckle region). In Thakur and Anand (2005) the most suitable wavelet shapes for ultrasound denoising – the DWT and wavelet packets method – are used according to the statistical significance test of the efficiency of the particular wavelet. Results are compared with the nonlinear adaptive filter scheme for speckle suppression. The peak signal-to-noise (PSNR) and normalized mean-square error (NMSE) are used to evaluate the results of the discrete wavelet methods.

This article investigates and compiles well-known techniques used in the smoothing or suppression of speckle noise in ultrasound images. A comparison of the methods studied is done based on an experiment, using quality metrics to test their performance and show the benefits each one can contribute. Similarly to Verhoeven and Thijssen (1993), the investigated digital filters were applied to computer simulated images.

The remainder of the paper is organized as follows. Section 2 introduces some explanations on digital speckle noise and presents the types of filters used in this study. Next, the methodology followed for assessing the performance on the reduction of speckle noise by the different approaches is described in Section 3. Section 4 shows the complete set of tests performed on the synthetic image. Lastly, some conclusions leading to finding out general tendencies in speckle noise reduction in ultrasound images are offered.

2. Speckle noise and some well-known filters

2.1. Types of noise

There are different types of noise in digital images. These are: impulsive or random noise, Gaussian noise, frequency noise and multiplicative noise. Impulsive noise can appear when the sensor that picks up the image is saturated and the value of the pixel shows a high value or when the signal is lost and the pixel shows a low value. In this case, the image has too high or too low pixel values. On the other hand, Gaussian noise shows little variation in the image for reasons such as different sensor gain, quantization errors in digitization, etc. At first sight, a noisy image appears to be the same as the original one but it is very different. Frequency noise is characterized by the interference of a signal which joins the image at a certain frequency. Lastly, multiplicative noise is the result of the multiplication of two signals. In all cases, noise always implies a sudden change in an image's intensity level; thus, noise is considered an image's high frequency component.

In the images this paper deals with, there is a characteristic type of noise called speckle noise. The images with this type of noise display a granular pattern due to the dispersion of the electromagnetic waves caused by the transducer. When the waves reflected on the rough texture make an impact on said texture, they create interferences which cause noise in the registered image. This noise is very harmful since it limits the detection of injuries, especially in low contrast images. To perfect the denoising methods, it is important to have an accurate and reliable model. This is not an easy task; however, the following model is considered a good model for images with speckle noise:

$$f(x,y) = g(x,y) \cdot \eta_m(x,y) + \eta_a(x,y) \tag{1}$$

In the previous formula $f(y,x)$ is the real noisy image, $g(x,y)$ represents an unknown noise-free image, which is what we are aiming for, $\eta_m(x,y)$ and $\eta_a(x,y)$ are multiplicative and additive noise functions. Since additive noise is considered to be lower than multiplicative noise, Loupas et al. (1989) proposed the following signal-dependent noise model for speckle specification in ultrasound images

$$f(x,y) = g(x,y) \cdot \eta_m(x,y) \tag{2}$$

2.2. Types of filters

The filters studied in this paper are:

(1) **Median filter**. This is a nonlinear filter applied to an image's spatial domain. The value of the median filter in suppression of impulsive noise has long been recognized. Median filtering (a standard pot-filtering technique) is often effective for speckle reduction. It uses the median intensity in a suitable sized and shaped region W_{ij} surrounding the pixel (i,j) of interest as the output pixel value; hence it eliminates any impulsive artifacts with an area (in pixels) less than half the region size $||W_{ij}||$ (Chen et al., 1996).

(2) **Adaptive weighted median filter**. The adaptive weighted median filter (AWMF) (Loupas et al., 1989) is an enhanced median filter. It introduces the concept of weighting coefficient for the pixels in the window. The coefficient affects every pixel in such a way that its value appears as many times as the weight in the estimation of the median indicates. Thus, if the weights are the same, this method will behave as a typical median filter. However, if the weights are not the same and they decrease from the centre of the window to the outer limits, the details and the edges of the image will be less altered. At the same time, less noise will be eliminated. Therefore, weight choice means compromising between noise suppression and image preserving. Bearing this in mind, the algorithm adapts the weights according to the image's characteristics in the area inside the window for each step of the image processing. The characteristics are determined by local statistical properties.

(3) **Fourier filtering**. Fourier filtering is, naturally, based on Fourier transform properties. In medical images, our objective is to find a filter or filtering function which will minimize Fourier transform's high frequency components. Once this is done, the output image will be obtained by means

of the inverse Fourier transform. We will consider two types of filters. One is known as ideal filter and the other one is Butterworth filter.

(4) **Wavelet transform**. With this transform we also obtain an input signal frequency representation. With a wavelet transform, we try to express a function in terms of small waves, thus the name wavelet. We are going to use a processing which can be carried out without implementing a very complex transform. It consists of eliminating certain frequencies in order to eliminate any existing noise. Since we know that when an image is decomposed, the HH, LH, and HL images contain most of the image's high frequencies and noise, we can eliminate the noise by eliminating those very images. This does not mean that all noise present in the image is eliminated. Some details in the image may also be lost. Recently it has been proposed some modifications to the original wavelet filtering (Chen, Bui, & Krzyżak, 2005; Chen & Kegl, 2007). However although these new techniques seem promising we are using the standard method.

(5) **Homomorphic filtering**. Speckle noise present in ultrasound images is considered multiplicative noise. This fact creates gaps in the previous methods since they are created, mainly, to eliminate random noise which occurs additively. Therefore, it seems logical to carry out a logarithmic transform on the original image, wherefore speckle noise becomes additive as is shown in the following equality:

$$\log f(x,y) = \log g(x,y) + \log \eta_m(x,y) \tag{3}$$

We now have an image without multiplicative noise which can be processed by traditional methods. At this point, we can choose from among several options, one of the most common being the application of a low pass filter in Fourier's domain. Fig. 1 shows a diagram of blocks with the process which is followed in the previous algorithm.

3. Proposed methodology

Noise suppression methods can be compared in one of two ways. In one, naturally, the different algorithms are placed in a collection of ultrasound images to obtain the corresponding smooth image. In this case, since we only have a noise corrupted image and the real noise-free image does not exist, conventional metrics cannot be used to indicate the quality obtained with filtering. We try, therefore, to give a subjective visual assessment of the algorithm's effect on the input image. Another way to compare the different methods consists of creating a synthetic image, taken as a noise-free image, and later applying the known noise models to corrupt it. Thus, smoothing techniques can be compared using numeric metrics, taking the noise-free image as a reference.

Another proposal is based on the fact that the current basic methods which are applied are few. Research relies on looking for variants and perfecting those techniques. In addition, we are also working on the combination of different techniques, as can be seen with homomorphic filtering. As an example of this, see Figs. 2 and 3, which show the process of the image in a diagram of blocks. Fig. 2 shows, basically, the diagram of the homomorphic filtering, but in this case, using the wavelet transform. On the other hand, Fig. 3 shows a more complex processing. Both methods are combined here: the AWMF algorithm and the wavelet coefficients processing. It also has another peculiarity, which is the fact that there are two ways of processing from one image.

Our purpose, based on these ideas, is to be able to build combinations from an input image with the basic methods. These combinations will be done in two different ways. On the one hand, there will be a sequence combination which will have a series of methods where the output of one will be the input of the next one. On the other hand, there is also a parallel combination made up of several sequence combinations. Thus, the resulting image from the whole process will be calculated as the average image of the resulting images of every sequence combination.

Sequence combinations are designed almost exclusively for the application of homomorphic filtering, performing a logarithmic transform at the beginning and an exponential transform at the end. Nevertheless, it is also open to cascading methods. We try to complement the positive and negative aspects of each sequence with a parallel combination, since the defects of one side will be compensated with the advantages of the other side, although each one's virtues will also diminish. To obtain the best possible results, a compromise will have to be made.

In this paper, the Field II (Jensen, 1996) program is used to simulate ultrasound images. The Field II program can simulate all kinds of ultrasound transducers and the associated images, and is extensively being used in other ultrasound image papers (e.g.

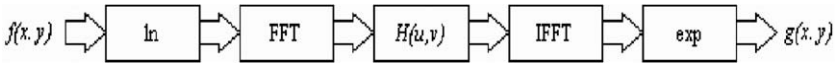

Fig. 1. Sequence of steps in homomorphic filtering example.

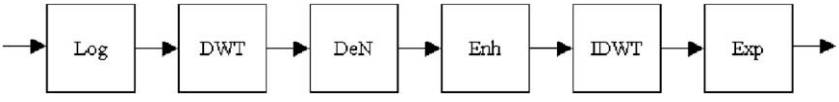

Fig. 2. Algorithm extracted from Zong et al. (1998).

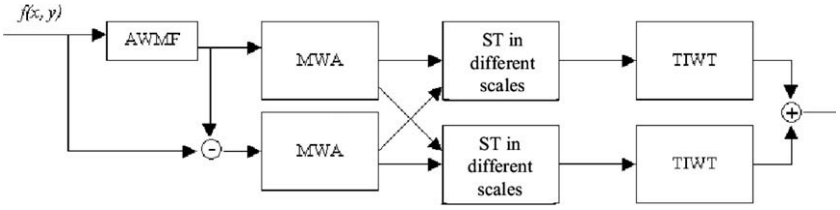

Fig. 3. Algorithm extracted from Hao et al. (1999).

Radulescu, Wójcik, Lewin, & Nowicki, 2003; Wang, Shen, & Wang, 2007; Xiao, Ng, Tsang, & Abeyratne, 2007). As in Adam et al. (2006), the study is performed by simulations processing B-mode images of a kidney. The Field program system uses the concept of spatial impulse responses as developed by Stepanishen (1971) and Tupholme (1969). The approach relies on linear systems theory to find the ultrasound field for both the pulsed and continuous wave case. This is done through the spatial impulse response. This response gives the emitted ultrasound field at a specific point in space as function of time, when the transducer is excited by a Dirac delta function. The field for any kind of excitation can then be found by just convolving the spatial impulse response with the excitation function. The impulse response will vary as a function of position relative to the transducer, hence the name spatial impulse response. The received response from a small oscillating sphere can be found by acoustic reciprocity. The spatial impulse response equals the received response for a spherical wave emitted by a point. The total received response in pulse-echo can, thus, be found by convolving the transducer excitation function with the spatial impulse response of the emitting aperture, with the spatial impulse response of the receiving aperture, and then taking into account the electromechanical transfer function of the transducer to yield the received voltage trace.

The metrics used to experiment with images have been the well-known mean-square error (MSE), signal-to-noise ratio (SNR), peak signal-to-noise ratio (PSNR), but also the so-called beta (β) metric proposed in Hao et al. (1999). The MSE, SNR and PSNR metrics are defined in the following expressions:

$$\mathrm{MSE} = \frac{1}{M \cdot N} \sum_{m=0}^{M-1} \sum_{n=0}^{N-1} \left[I(m,n) - \widehat{I}(m,n) \right]^2 \tag{4}$$

$$\mathrm{SNR} = 10 \cdot \log_{10} \frac{\frac{1}{M \cdot N} \sum_{m=0}^{M-1} \sum_{n=0}^{N-1} I^2(m,n)}{\mathrm{MSE}} \tag{5}$$

$$\mathrm{PSNR} = 10 \cdot \log_{10} \frac{255^2}{\mathrm{MSE}} \tag{6}$$

In these expressions, I is the original image and $\widehat{I}$ is the estimation of the original image obtained from a noisy image. The images' measurements are $M \cdot N$.

Beta metric is defined as

$$\beta = \frac{\sum_{m=0}^{M-1} \sum_{n=0}^{N-1} \left[\Delta I(m,n) - \overline{\Delta I} \right] \cdot \left[\Delta \widehat{I}(m,n) - \overline{\Delta \widehat{I}} \right]}{\sqrt{\sum_{n=0}^{N-1} \left[\Delta I(m,n) - \overline{\Delta I} \right]^2 \cdot \left[\Delta \widehat{I}(m,n) - \overline{\Delta \widehat{I}} \right]^2}} \tag{7}$$

where the Δ operator means applying a high pass filter to the image. To perform the filtering, the Laplacian operator is used in its 3×3 version. $\overline{Delta}$ is the mean value of the image after the operator is applied.

The MSE metric indicates how different the images being compared are. Therefore, the lower its value is, the closer the estimated image is to the original image and the better performance the algorithm, which was used to obtain the estimation, has. However, the SNR and PSNR metrics show a relationship between the real image and the estimation error. Here, a high value indicates an improvement. The beta metric is used to evaluate the preservation of the edges in the estimated image. In this case, an increase of this parameter also indicates better performance qualities.

4. Data and results

To compare the algorithms, we will start with the kidney image in Fig. 4a. From this image, we have generated a noisy image (see Fig. 4b) using the Field II program previously described. The values obtained from the metrics for this image are presented in Table 1.

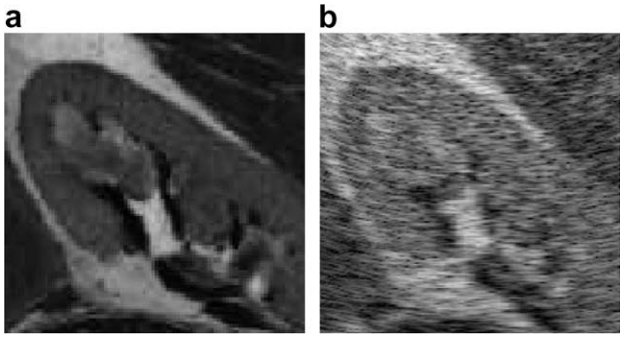

Fig. 4. (a) Reference image for the comparison. (b) Noisy image.

4.1. Median filter

Different window sizes have been used for this algorithm. To be exact, we have used sizes 3, 5, 7, 9 and 11 and the values obtained are those presented in Table 2.

Notice that in the table, according to the metrics, a median filter with a 3×3 window size eliminates noise in such a way that we obtain a better quality image than the noisy image. In this case, all values indicate this improvement. This tendency continues as the window size increases (see Table 2.

This evolution is clearly seen in Fig. 5. In this figure, we see the images generated with the median filter for each window size. In (a) the size of the window is 3×3, in (b) 5×5, in (c) 7×7, in (d) 9×9, and in (e) 11×11. In this figure, we see, gradually, how as the window size increases, the image gets smoother and the colors get more uniform. For example, at a glance, the image obtained by applying a filter size 11 hardly shows variations in the background of the white area in the upper left corner of the image.

In contrast, the damaging effects are more visible. In the first image, the borders are still well defined. But from image (b) on, and as the window size increases, the borders get more and more blurry. This effect increases with every step, especially in the white central rectangular zone.

To sum up, if we use a small window (3×3) with this method, we can make some of the noise disappear, without losing important details. But if the size of the window is increased to eliminate more noise, we get a counter-productive effect which results in the loss of edges. Small details in the image can also disappear.

4.2. Adaptive weighted median filter

After testing the median algorithm, we continue with the adaptive weighted median algorithm (AWMF). This algorithm is more

Table 1
Metrics values for noisy image.

MSE	SNR	PSNR	β
1825.285599	3.121050	15.517495	0.012505

Table 2
Metrics obtained when applying the median filter.

Window	MSE	SNR	PSNR	β
3×3	1652.592804	3.552700	15.949145	0.018514
5×5	1528.061813	3.892949	16.289394	0.034675
7×7	1459.290619	4.092941	16.489386	0.041750
9×9	1413.899063	4.230175	16.626620	0.055058
11×11	1384.809921	4.320457	16.716902	0.062093

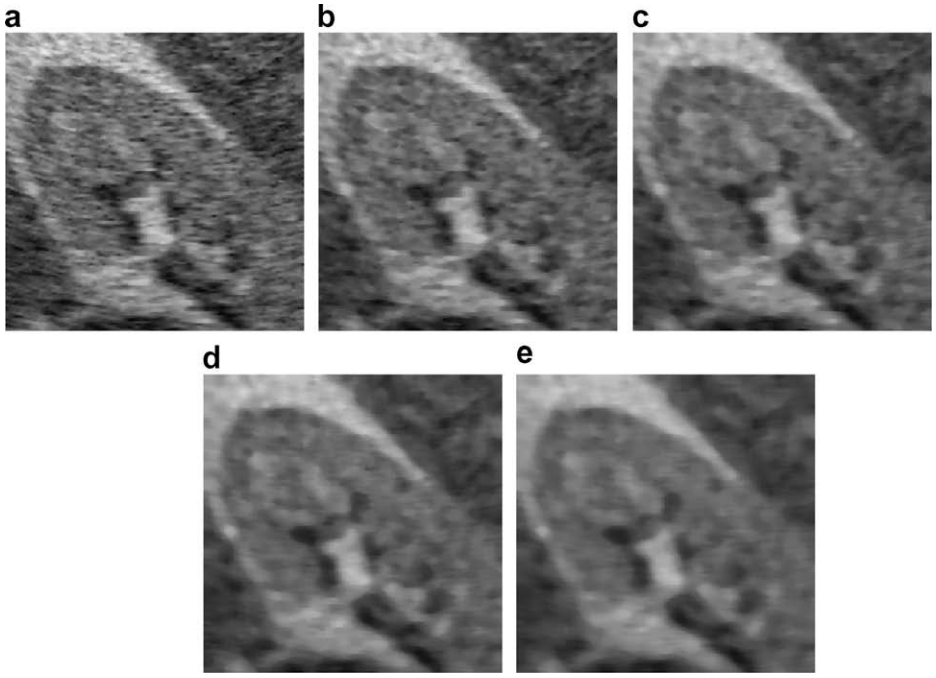

Fig. 5. Images after applying the median filter with different window sizes. (a) 3×3 window. (b) 5×5 window. (c) 7×7 window. (d) 9×9 window. (e) 11×11 window.

complex than the previous one because it tries to adapt to the image's conditions to minimize noise, as much as possible, without losing image quality. This also makes its use more difficult since we have to deal with a three-parameter space to apply the algorithm. These parameters are the window size and the formula's c_1 and c_2 scalar variables

$$w_{ij} = c_1\left(1 - c_2\frac{d}{(\mathrm{SNR})^2}\right) \tag{8}$$

where d is the Euclidean distance from the (i,j) position to the centre of the window, c_1 and c_2 are weight adjustment constants and SNR indicates the relationship between the mean and the standard deviation of the pixels which fall inside the window. The SNR value is used to find out what the image in the area of the window is like. If the SNR value is high, it means that the image is very uniform and the noise in this area is what causes the small variation in the pixels' values. The weights are, therefore, very similar and are adjusted to perform a very aggressive filtering, since there is no risk of eliminating important details from the image. If, on the other hand, SNR has a low value, it means that the deviation is great, which indicates that there is an abrupt change in the pixels' values just like when there are edges or other small details. In this case, the weights are big in the centre of the window and decrease at the outer edges, thus getting a less aggressive filtering which preserves these important elements.

To get good use, we must first set the values for those parameters and then, depending on the results, change them according to what each one means. Just as with the median filter, window size influences the amount of noise eliminated, as well as the details in the real image. Variable c_2 is used to control the importance of the distance to the centre of the window. Great values make the far away pixels seem less important. Variable c_1 is applied over all weights equally, thus its mission is to highlight the differences. This means that, if this variable increases in a certain situation, the distances between weights become greater and these weights will condition the median's general value the most. For example, if little noise is eliminated with a configuration, due to the little consideration given to the outside pixels, when c_1 increases less noise will usually be eliminated. This is so because, if the centre pixel was already the heaviest, in the new situation it will be even farther away from the rest.

4.2.1. First series of tests

In Table 3, the values obtained for the tests with the adaptive weighted median filter are summed up, starting with the values indicated in Loupas et al. (1989). They are 11 for window size, 99 for c_1 and 10 for c_2.

Fig. 6 shows the same results in an image.

There is no significant improvement in $c_1 = 99$, although all metrics improve. At a glance, the processed image really looks like the noisy image, as could be guessed by the metrics. After this first approximation, variable c_1's value can continue to decrease up to 50. There is an overall improvement but this improvement contributes little since the image is almost the same, as we can see in Fig. 6b. However, since this seems to be a way to reduce noise, c_1's value can continue to decrease. We now try with value 20 and get the metrics shown in Table 3. The tendency to improve image quality continues concerning metrics about noise reduction (MSE, SNR and PSNR), however we get a worse value for β metric so this fact we near an inflexion point and we cannot obtain better images reducing c_1 parameter.

4.2.2. Second series of tests

Instead of keep on reducing c_1 parameter we can move onto other parameter like window size. To do this we have fixed c_1 to 20 and c_2 to 5, and we have tested two window sizes, 11 and 17. The resulting images can be seen in Fig. 6d and 6e, and the numeric

Table 3
Metrics obtained when applying the adaptive weighted median filter in function of parameter c_1 for a window size of 11 and $c_2 = 10$.

c_1	MSE	SNR	PSNR	β
99	1823.777542	3.124640	15.521085	0.012393
50	1805.582321	3.168186	15.564631	0.012814
20	1780.537109	3.228848	15.652930	0.012210

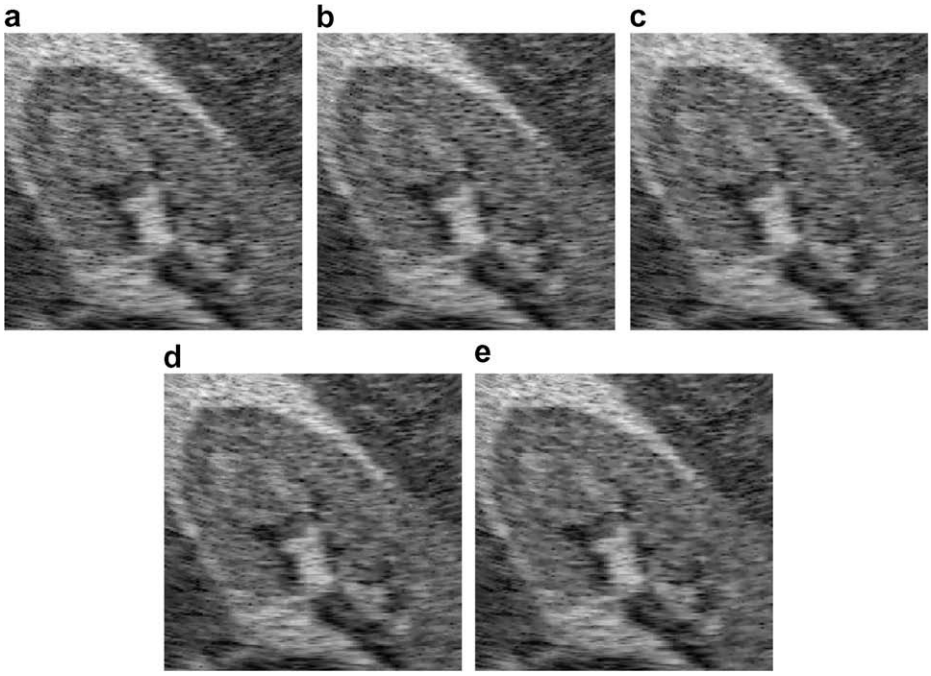

Fig. 6. Images after applying the AWMF filter with different configurations. (a) 11-99-10. (b) 11-50-10. (c) 11-20-10. (d) 11-20-5. (e) 17-20-5.

results are shown in Table 4. Here the numbers say us that increasing window size allow us to remove more noise in the image but we get worse edges. This conclusion is similar to the one obtained with Median filter.

4.2.3. Third series of tests

In view of these results, we try to lower parameter c_1 much more to see if the quality improves. c_2's value will also be lowered. The purpose is to weigh more those pixels farthest away from the one we are dealing with, in order to eliminate more noise. The results of these new experiments are shown in Fig. 7a–c and Table 5.

The metrics for the image obtained with the AWMF algorithm, with parameter size equal to 11, c_1 equal to 1 and c_2 equal to 1 are shown first. Notice that the predictions were correct and the noise has been eliminated even more because the MSE metric has been reduced and the SNR and PSNR metrics have increased. At the same time, we have not only not lost precision in the edges, but we have improved them greatly. The image obtained in this process is shown in Fig. 7a. This image enhances highly according to the metrics, but visually we can appreciate that the borders appear blurred. On the other hand, the variations in color, typical of noise, are not noticeable.

Since these values have proved to yield good results, we can continue to increase parameter c_1 to try to improve further. For instance, we decide to set c_1's value to 2, thus obtaining the metrics. The resulting image, after applying the algorithm with these parameters, is shown in Fig. 7b. Visually this new image and the

Table 4
Metrics obtained when applying the adaptive weighted median filter in function of parameter window size and $c_1 = 20$ and $c_2 = 5$.

Window	MSE	SNR	PSNR	β
11	1743.153946	3.321001	15.717446	0.018874
17	1734.902267	3.341609	15.738053	0.017285

Table 5
Metrics obtained when applying the adaptive weighted median filter in function of parameter c_1 for a window size of 11 and $c_2 = 1$.

c_1	MSE	SNR	PSNR	β
1	1380.900772	4.332734	16.729179	0.052046
2	1388.240372	4.309712	16.706157	0.051380
3	1716.154694	3.388794	15.785239	0.019028

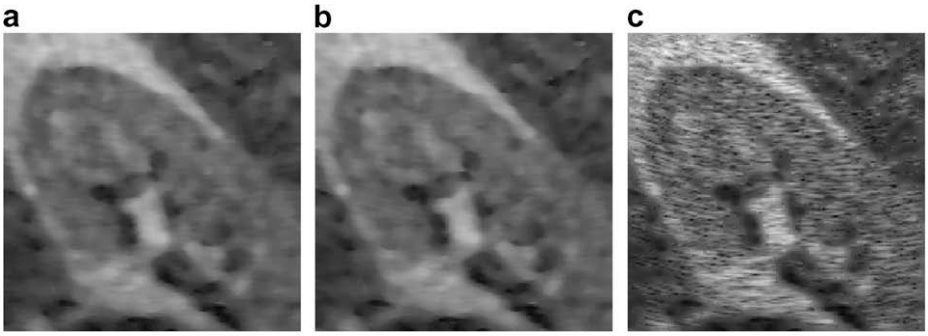

Fig. 7. Images after applying the AWMF filter with different configurations. (a) 11-1-1. (b) 11-2-1. (c) 11-3-1.

last one look similar, however, with this change, we have lost a little of quality in every aspect, from noise suppression to edge improvement, but the difference is hardly notable. Although it seems that increasing c_1 yields poorer results we try another configuration with $c_1 = 3$. With this configuration, we have obtained a very different image as can be seen in Fig. 7c. In this case, the metrics values shown that this last configuration is worse, the filter has removed much less noise.

After seeing the results of the AWMF algorithm on this image, we can deduce that the best way to obtain the best image after processing is the 11-1-1 configuration. The reason is that the resulting image is the most similar to the original image, since it has the lowest MSE metric value and a very high beta metric value. If we interpret the meaning of c_1 and c_2, when we set these two parameters to 1 the filter behaves quite similar like Median filter with the same window size. This is corroborated by the results and taking that into account we can conclude that AWMF cannot improve the results of the Median filter for the same window size.

4.3. Fourier filtering

4.3.1. Ideal filter

We now go on to evaluate the Fourier filtering using an ideal filter. The evaluation process is now easier because we have to move only through one parameter, which is the cutoff frequency. The results are shown in Fig. 8 and Table 6.

First, the cutoff frequency will be set at 10%. By looking at the metric values, we can already tell that this image is of much better quality than the noisy image because all values indicate so. Looking at the image, we see that the noise in some parts of the background is smoother but the objects contours have become blurred and there is a wave effect around the line and the rectangle. This is known as the Gibbs effect. If the algorithm cutoff off value were lowered even more, we would get greater smoothness but we would also lose sharpness in the image and the Gibbs effect would become more significant. That is why we do not lower the cutoff value any more. On the contrary, it will be raised to avoid these damaging effects.

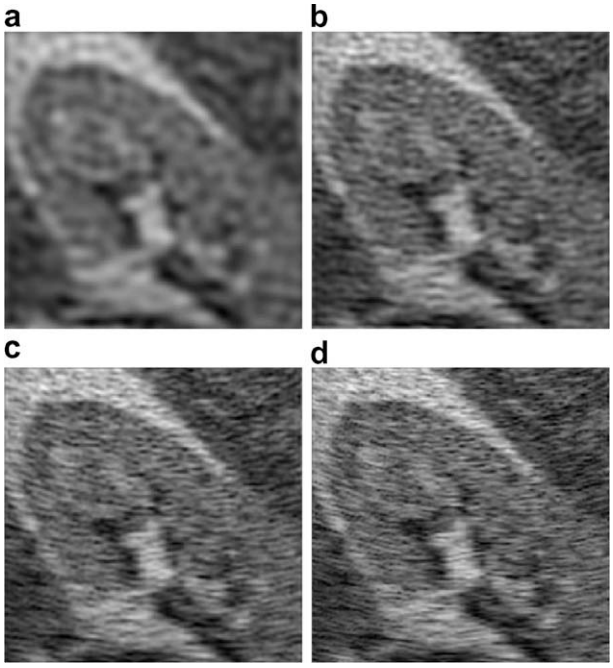

Fig. 8. Images after applying the Fourier ideal filter with different cutoffs. (a) 10%. (b) 20%. (c) 30%. (d) 40%.

Thus, situating the cutoff value at 20%, the values indicate that there has been improvement with regard to the noise image but, of course, not with the previously filtered image, as you may appreciate by the big descent (about a 50%) of the β value. In Fig. 8b, this new image is shown and we notice that we have obtained some sharpness with regard to the previous one and the Gibbs effect is slightly lower. On the negative side, we see that there is less color uniformity. The cutoff value will now be set at 30%. Just as we expected, the data show that there is an improvement in image quality with respect to the noisy image. The MSE metric has increased with regard to the previous image. Looking at the image in Fig. 8c, we see that the Gibbs effect has now disappeared. This means a higher contrast or, in other words, a higher frequency. If we apply a filter with a 40% cutoff value, the quality of the filtered image is worse than before. This is corroborated by the metric values.

4.3.2. Butterworth filter

These previous results belonged to an ideal filter, which means a sharp cut off in the frequencies. The Butterworth filter tries to smooth this cut off and eliminate the Gibbs effect and the excessive minimizing of high frequency image details at the expense of losing noise elimination capacity. Table 7 shows the metrics for the images generated with this filter (Fig. 9).

As we have done previously, the Butterworth filter will be first set at a cutoff value of 10% to start evaluating its results. This image, shown in Fig. 9a, has better metrics than the noisy image and even more so than the image obtained with an ideal filter with the same cutoff value, except for β parameter. Here β is reduced although the Gibbs effect does not appear. This is so, because there is not sharp cut off in the frequency coefficients, as with an ideal filter. A negative side of this is that the objects are a little blurred. This effect was not as evident in the previous images because it was masked by the Gibbs phenomenon.

As before, we will analyze that it is not possible to obtain more quality by raising the cutoff value, and in this case, setting it at 20%. According to the MSE, SNR and PSNR metrics, with this cutoff value, you get a worse image than the previous one and, relatively speaking, the loss in quality is similar to that obtained with an ideal filter with the same cut off values.

Nevertheless, there is something which does not seem logical for a beta parameter, which is edge deterioration. This does not fit in accord with reality because in Fig. 9b this image is shown and the objects are better defined and less blurred. This lack of agreement between the numeric data and observation can only be explained by the fact that increasing the cutoff value allows more noise to enter the image, which in turn, affects the edges. Thus, the increase in sharpness is compensated with the greater

Table 6
Metrics obtained when applying the Fourier ideal filter.

Cutoff (%)	MSE	SNR	PSNR	β
10	1466.367798	4.071930	16.468374	0.073053
20	1591.829346	3.715394	16.111839	0.033076
30	1685.922241	3.465983	15.862428	0.025595
40	1748.550690	3.307576	15.704021	0.020017

Table 7
Metrics obtained when applying the Butterworth filter.

Cutoff (%)	MSE	SNR	PSNR	β
10	1423,568420	4,200575	16,597020	0,040237
20	1510,383530	3,943486	16,339931	0,025541
30	1580,116333	3,747468	16,143913	0,019615
40	1632,239960	3,606519	16,002964	0,016608

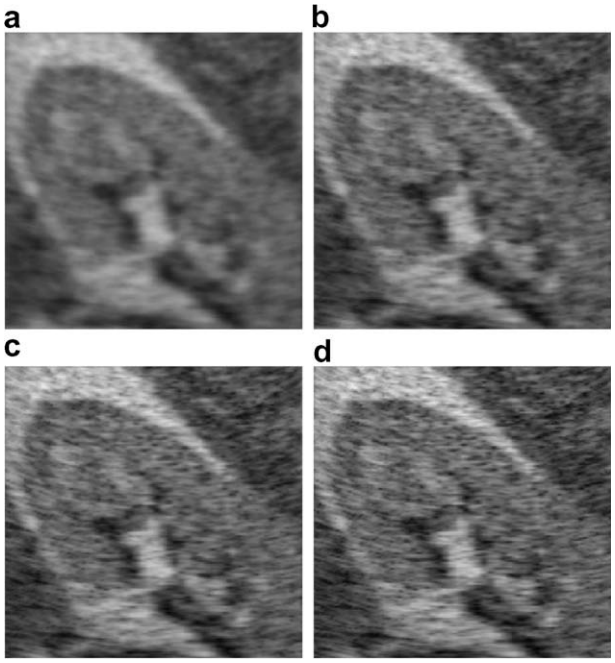

Fig. 9. Images after applying the Butterworth filter with different cutoffs. (a) 10%. (b) 20%. (c) 30%. (d) 40%.

Table 8
Metrics obtained when applying the wavelet filter in function of the band eliminated with a decomposition level of 1.

Band	MSE	SNR	PSNR	β
HL	1821.261490	3.130636	15.527081	0.013653
LH	1720.212020	3.378463	15.774908	0.019281
HH	1823.779022	3.124637	15.521081	0.014292

irregularity given by noise. At any rate, the beta metric value indicates an improvement with regard to the unprocessed image, which was expected.

Continuing with the process of raising the cutoff value, the next step is to set it at 30%. We obtain this table with the metrics. The same changes as before take place here. That is, MSE, SNR and PSNR metrics indicate a loss in image quality and a continuation in the decrease of the beta metric. The image belonging to this configuration is shown in Fig. 9c.

We will now test this filter with a cutoff value of 40%. The table shows the same evolution in the numbers. Fig. 9d shows the image for this test. Here, it is not possible to see, at a glance, any point which differs from the previous image.

After taking a look at these cases with a Fourier filter, we can say that an ideal filter is not very satisfactory, since the Gibbs effect appears. This effect distorts the image very much, more so, the lower the cutoff value is. On the other hand, this effect does not exist with a Butterworth filter and the image can be smoother. Even so, the results obtained with an AWMF algorithm can be improved with this filter.

4.4. Wavelet filtering

4.4.1. First series of tests

Next, we will take a look at the wavelet filtering. The results of a first series of tests are shown, as a table, in Table 8 and as images in Fig. 10a–c.

As a first approach to this algorithm, we will only eliminate bands in a single decomposition level with at least one high frequency component (HL, LH and HH). Theoretically these bands contains more noise, specially band HH. The filtered images are shown in Fig. 10a, b and c. According with the metrics the best

Table 9
Metrics obtained when applying the wavelet filter in function of the bands and the decomposition level.

Level/bands	MSE	SNR	PSNR	β
2/HL	1813.258606	3.149761	15.546206	0.014232
2/LH	1596.462051	3.702773	16.099218	0.014953
2/HH	1814.264099	3.147254	15.543799	0.014793
2/LH,HH	1583.939026	3.736974	16.133419	0.019704

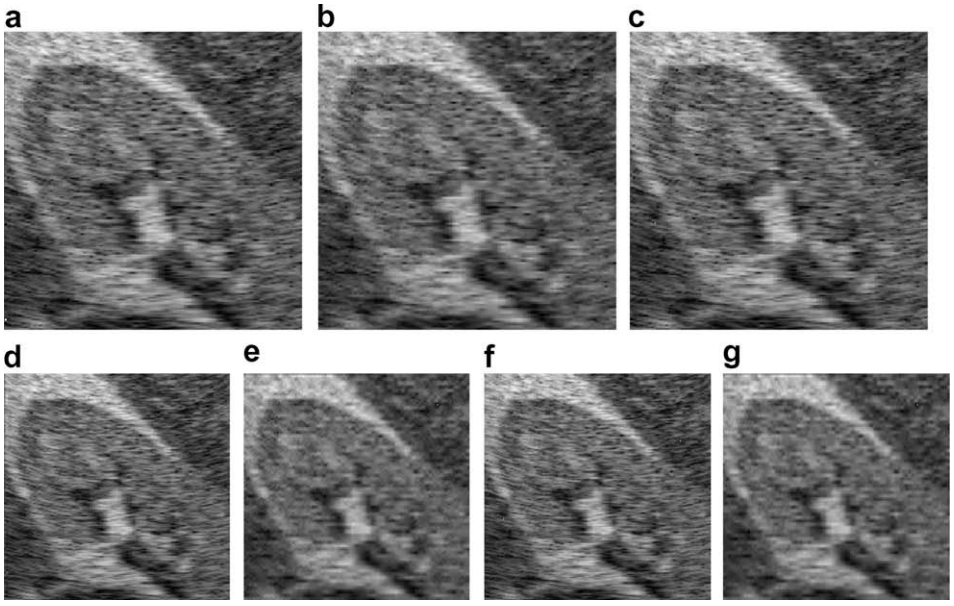

Fig. 10. Images after applying the wavelet filter for different configurations. (a) 1 level and band HL. (b) 1 level and band LH. (c) 1 level and band HH. (d) 2 levels and band HL. (e) 2 levels and band LH. (f) 2 levels and band HH. (g) 2 levels and bands LH and HH.

Table 10
Metrics obtained when applying the homomorphic filter to the AWMF filter.

	MSE	SNR	PSNR	β
11-90-10	1826.764069	3.117534	15.513979	0.009380
11-50-10	1826.797424	3.117455	15.513900	0.009319
11-20-10	1824.668442	3.122519	15.518964	0.009911
11-20-5	1828.368851	3.113731	15.510165	0.008657
17-20-5	1830.939178	3.107620	15.504064	0.017923
11-1-1	1384.809921	4.320457	16.716902	0.062093
11-2-1	1384.809921	4.320457	16.716902	0.062093
11-3-1	1817.576874	3.139431	15.535876	0.010062

Table 11
Metrics obtained when applying the homomorphic filter to the Fourier filter.

	MSE	SNR	PSNR	β
Ideal 10%	1326.001465	4.508919	16.905364	0.076284
Ideal 20%	1516.865936	3.924887	16.321332	0.031131
Ideal 30%	1654.623245	3.473670	15.943812	0.022885
Ideal 40%	1746.871048	3.311750	15.708195	0.015925
Butterworth 10%	1185.161743	4.996582	17.393027	0.038180
Butterworth 20%	1358.763123	4.402921	16.799366	0.024359
Butterworth 30%	1470.699249	4.059120	16.455565	0.018131
Butterworth 40%	1549.100906	3.833562	16.230007	0.016088

way to improve the noisy image is to remove LH band. Looking at the images we can see that in images processed with HL and HH bands appears some white spots which are not in the original image, so this fact deteriorate the metric results.

In other hand we know that band LH contain high frequency for horizontal edges and the tested image has more vertical edges than horizontal (although most of the lines are diagonal), so if we remove this band we remove lot of noise but not much edges information.

4.4.2. Second series of tests

Since the best choice, up to now, is to eliminate the LH band but in one decomposition level, we can try now with a second level. The results are shown in Table 9 and Fig. 10d–g.

In this table we can see that we get better results compared with one level processing, specially with LH band but not with β metric which has decreased a lot. Looking at the image we can guess that this fact can be explained because now appear the white spots.

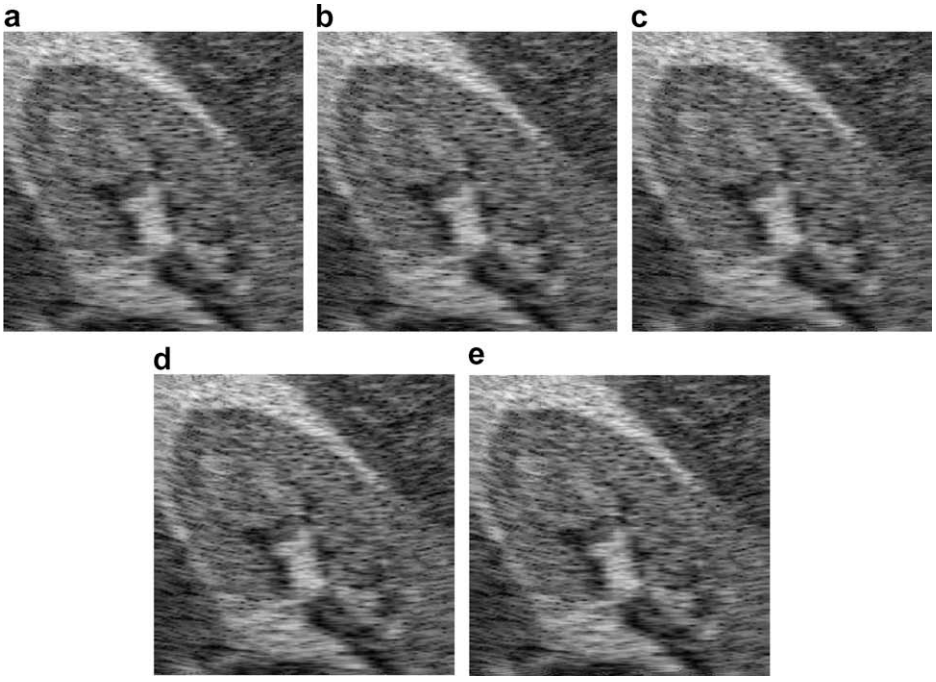

Fig. 11. Images after applying the homomorphic filter to the AWMF algorithm with parameters (a) 11-90-10, (b) 11-50-10, (c) 11-20-10, (d) 11-20-5, (e) 17-20-5.

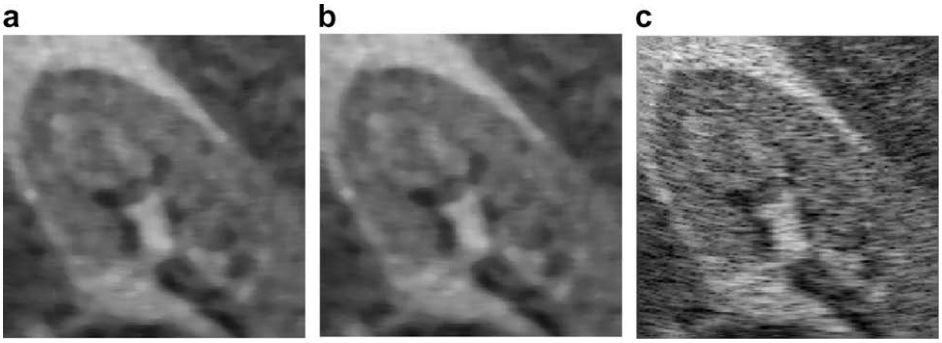

Fig. 12. Images after applying the homomorphic filter to the AWMF algorithm with parameters (a) 11-1-1, (b) 11-2-1, and (c) 11-3-1.

We have tested a new filtered image obtained by removing band LH and HH in the second level. The metrics results are also in Table 9, which shown that this combination gets a better image specially in β metric, however in the image still appear the white spots.

4.5. Homomorphic filtering

The same tests, with the same parameters have been used with each algorithm using the homomorphic filtering diagram, except for the median filter diagram. This exception has been made because using the homomorphic filtering with the median filter as a nucleus would not change anything, as opposed to applying only the median filter, since it is based on the existing order relationship between the pixels in an image. Thus, applying the logarithm to each one would not change this specific order.

4.5.1. AWMF filter

We will now go on to the AWMF filter. The results for the metrics obtained in each case for this filter are shown in Table 10. In

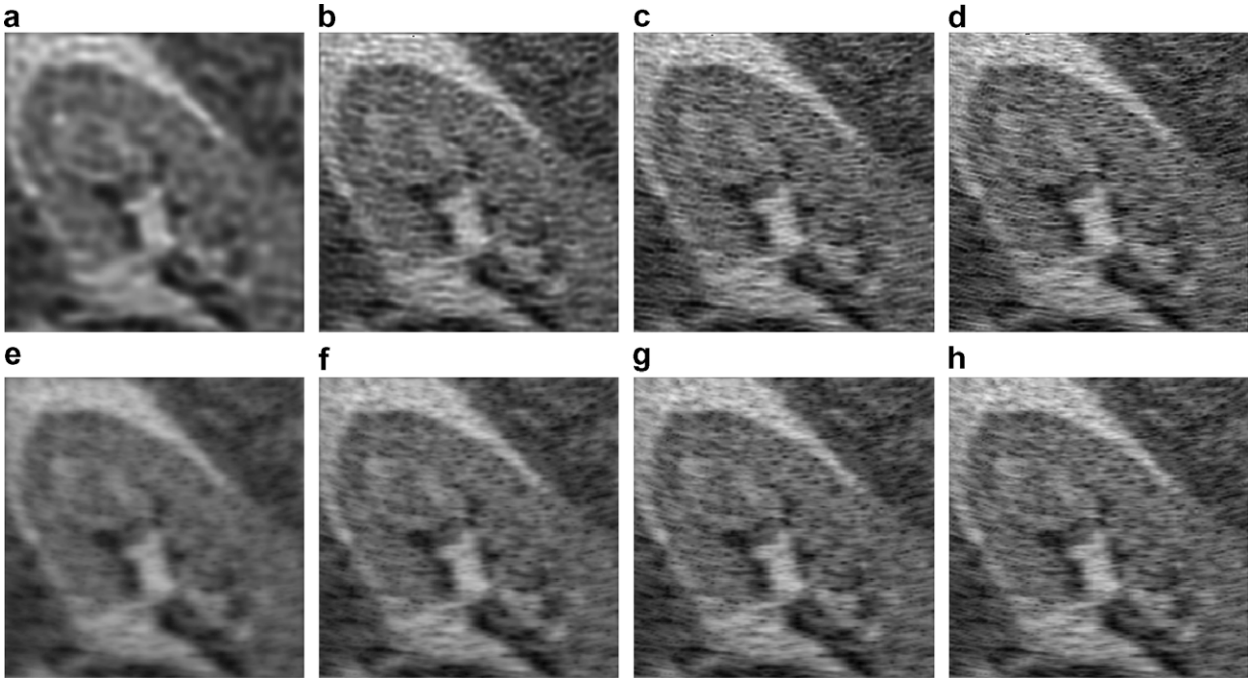

Fig. 13. Images after applying the homomorphic filter to the ideal Fourier filter (a) 10%, (b) 20%, (c) 30%, (d) 40%. Images after applying the homomorphic filter to the Butterworth filter (a) 10%, (b) 20%, (c) 30%, (d) 40%.

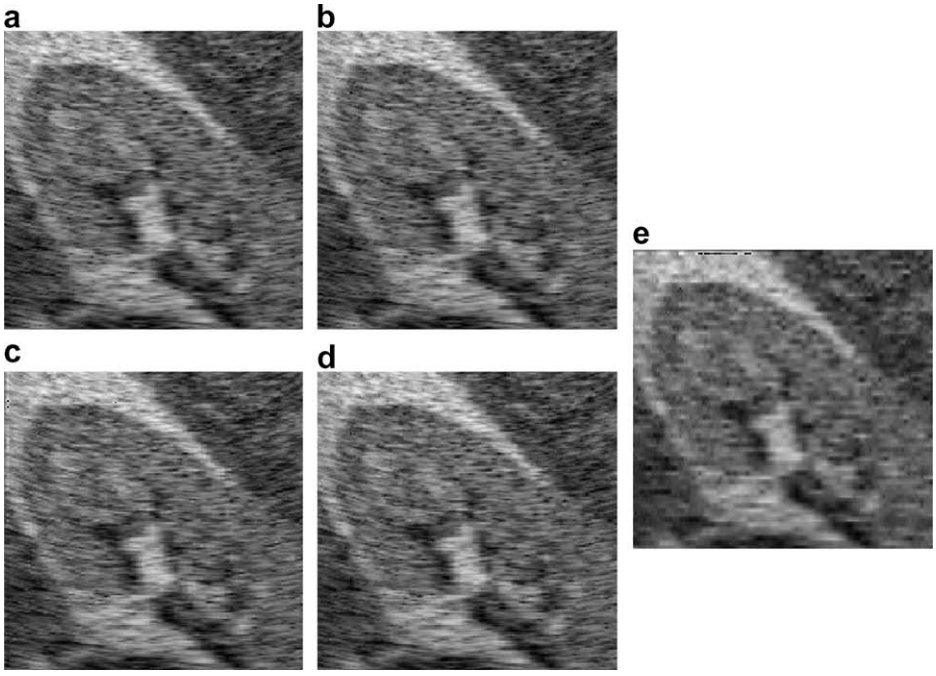

Fig. 14. Images after applying the homomorphic filter to the wavelet filter (a) 2 levels and band HL. (b) 2 levels and band LH. (c) 2 levels and band. (d) 2 levels and bands LH and HH.

Table 12
Metrics obtained when applying the homomorphic filter to the wavelet filter.

	MSE	SNR	PSNR	β
Level 1/HL	1821.985611	3.128909	15.525354	0.012872
Level 1/LH	1702.802963	3.422715	15.819160	0.017351
Level 1/HH	1823.531799	3.125225	15.521670	0.013359
Level 2/HL	1817.533997	3.139533	15.535978	0.014185
Level 2/LH	1530.535309	3.885925	16.282370	0.018517
Level 2/HH	1817.079117	3.140620	15.537065	0.013741
Level 2/LH,HH	1510.758530	3.942408	16.338853	0.022574

this table, the results are shown in the same order as when the AWMF filter was shown. If this table is compared with the results shown previously, we see that practically all metrics are worse, except for the configuration 11-2-1. The images generated with these parameters are shown in Figs. 11 and 12.

It seems that using a homomorphic filtering with this algorithm is not a good choice. The reason is that by transforming the input image with the logarithm function, the distance between the image's intensity values is reduced and it is more difficult to distinguish between noise and borders. Besides, it is needed to use a configuration of parameters more aggressive in order to obtain similar results without homomorphic filter. This could be the reason why there is no use of homomorphic filtering with the AWMF filter in the bibliography.

Nevertheless, it is very common to find the Fourier filtering being used as the nucleus of the homomorphic filtering. This is expected to work well and it can be seen in our experiments, as shows Table 11, where we see the metrics for the images obtained using a homomorphic filtering with the Fourier filtering (see also Figs. 13). Better results are obtained in every case, opposite as before. Only it has to be pointed out that, apart from ideal filter with 10% as cut off, in all cases β values are worse.

4.5.2. Wavelet filtering

Now, the only thing left is to test the homomorphic filtering with the wavelet filtering. Table 12 shows the results obtained in this case. The corresponding images may be found in Figs. 14. Here, if we compare the results with the ones shown earlier for the wavelet filtering, we notice that there are some cases where homomorphic filter gets better results and some others which are the opposite. However we can see that the cases where we can get better results with homomorphic filter are those which previously were better (1/LH, 2/LH and 2/LH,HH).

5. Conclusions

In this paper, we have tried to deal with the biggest problem regarding the processing of medical images: noise. Images in the medical field, such as magnetic resonance imaging, X-rays, ultrasound images, etc. are a very significant tool for the diagnosis and study of various illnesses. Given the growing importance of their use, these images have to be as sharp as possible. Even so, in some cases all the help possible is needed to interpret the images. This paper has focused on ultrasonic images or ultrasound images and more specifically, on the suppression methods of the characteristic noise in this type of images: the so-called speckle noise.

In this respect, this paper has compared some of the different algorithms and methods currently used to smooth the existing noise in medical images obtained through ultrasound images. We have explained a whole series of methods used in this field. The comparative study of noise suppression methods in ultrasound images was carried out on a noise-free synthetic image. We have used the Field II software to corrupt the image, adding the typical noise in ultrasound images. Afterwards we have shown some of the most common smoothing techniques over this image using numeric metrics, taking the noise-free image as a reference.

The first conclusion is that the best quality images are obtained with Fourier filter. The others can provide some improvement, but not that much. Besides, using Fourier filter is much more simple than any of the others because it only takes one parameters. However, AWMF has three parameters and it does not yield results as good as Fourier filter does.

The wavelet filtering, as we have seen, does not seem recommendable with real ultrasound images. It not only does not eliminate a lot of noise, but when the bands are eliminated, an effect with white dots appears that distorts the image very much. The homomorphic filtering should be only used with Fourier filter, however with the other filters it is not that useful.

References

Abd-Elmoniem, K. Z., Youssef, A. B., & Kadah, Y. M. (2002). Real-time speckle reduction and coherence enhancement in ultrasound imaging via nonlinear anisotropic diffusion. *IEEE Transactions on Biomedical Engineering, 49*(9), 997–1014.

Adam, D., Beilin-Nissan, S., Friedman, Z., & Behar, V. (2006). The combined effect of spatial compounding and nonlinear filtering on the speckle reduction in ultrasound images. *Ultrasonics, 44*(2), 166–181.

Bamber, J. C., & Daft, C. (1986). Adaptive filtering for reduction of speckle in ultrasonic pulse-echo images. *Ultrasonics, 24*(1), 41–44.

Behar, V., Adam, D., & Friedman, Z. (2003). A new method of spatial compounding imaging. *Ultrasonics, 41*(5), 377–384.

Bernstein, R. (1987). Adaptive nonlinear filters for simultaneous removal of different kind of noise in images. *IEEE Transactions on Circuits and Systems, 34*(11), 1275–1291.

Chen, Y., Broschat, S., & Flynn, P. (1996). Phase insensitive homomorphic image processing for speckle reduction. *Ultrasonic Imaging, 18*(2), 122–139.

Chen, G. Y., Bui, T. D., & Krzyżak, A. (2005). Image denoising with neighbour dependency and customized wavelet and threshold. *Pattern Recognition, 38*(1), 115–124.

Chen, G. Y., & Kegl, B. (2007). Image denoising with complex ridgelets. *Pattern Recognition, 40*(2), 578–585.

Chen, Y., Yin, R., Flynn, P., & Broschat, S. (2003). Aggressive region growing for speckle reduction in ultrasound images. *Pattern Recognition Letters, 24*(4-5), 677–691.

Donoho, D. L. (1995). De-noising by soft-thesholding. *IEEE Transactions on Information Theory, 41*(3), 613–627.

Hao, X., Gao, S., & Gao, X. (1999). A novel multiscale nonlinear thresholding method for ultrasonic speckle reduction. *IEEE Transactions on Medical Imaging, 18*(9), 787–794.

Huang, Q. H., & Zheng, Y. P. (2006). An adaptive squared-distance-weighted interpolation for volume reconstruction in 3D freehand ultrasound. In *Proceedings of Ultrasonics International (UI'05) and World Congress on Ultrasonics (WCU). Ultrasonics*, *44*(Supplement 1), e73–e77.

Huang, Q. H., Zheng, Y. P., Lu, M. H., & Chi, Z. R. (2005). Development of a portable 3D ultrasound imaging system for musculoskeletal tissues. *Ultrasonics, 43*(3), 153–163.

Jensen, J. A. (1996). Field: A program for simulating ultrasound systems. In *10th Nordic-Baltic Conference on Biomedical Imaging* (1). *Medical and Biological Engineering and Computing*, *4*(Supplement 1). 351–353.

Jespersen, S., Wilhjelm, J., & Sillese, H. (1998). Multi-angle compounding imaging. *Ultrasonic Imaging, 20*(2), 81–102.

Karaman, M., Kutay, M. A., & Bozdagi, G. (1995). An adaptive speckle suppression filter for medical ultrasonic imaging. *IEEE Transactions on Medical Imaging, 14*(2), 283–292.

Kotropoulos, C., & Pitas, I. (1992). Optimum nonlinear signal detection and estimation in the presence of ultrasonic speckle. *Ultrasonic Imaging, 14*(3), 249–275.

Loupas, T., McDicken, W., & Allan, P. (1989). An adaptive weighted median filter for speckle suppression in medical ultrasound images. *IEEE Transactions on Circuits and Systems, 36*(1), 129–135.

Radulescu, E. G., Wójcik, J., Lewin, P. A., & Nowicki, A. (2003). Nonlinear propagation model for ultrasound hydrophones calibration in the frequency range up to 100 MHz. *Ultrasonics, 41*(4), 239–245.

Rakotomamonjy, A., Deforge, P., & Marche, P. (2000). Wavelet-based speckle noise reduction in ultrasound B-scan images. *Ultrasonic Imaging, 22*(2), 73–94.

Sanches, J. M., & Marques, J. S. (2003). A MAP estimation algorithm with Gibbs prior using an IIR filter. *Energy Minimization Methods in Computer Vision and Pattern Recognition, Lecture Notes in Computer Science, 2683*, 436–449.

Stepanishen, P. R. (1971). The time-dependent force and radiation impedance on a piston in a rigid infinite planar baffle. *Journal of the Acoustic Society of America*, 49 841–849.

Stetson, P., Graham, F., & Macovski, A. (1997). Lesion contrast enhancement in medical ultrasound imaging. *IEEE Transactions on Medical Imaging, 16*(4), 416–425.

Stippel, G., Philips, W., & Lemahieu, I. (2002). A new denoising technique for ultrasound images using morphological properties of speckle combined with tissue classifying parameters. In *Conference Proceedings of SPIE Medical Imaging 2002*, Vol. 4687. pp. 324–333.

Thakur, A., & Anand, R. S. (2005). Image quality based comparative evaluation of wavelet filters in ultrasound speckle reduction. *Digital Signal Processing, 15*(5), 455–465.

Tolba, T. S. (2002). Wavelet packet compression of medical images. *Digital Signal Processing, 12*(4), 441–470.

Trahey, G., Smith, S., & Van Ramm, O. (1986). Speckle pattern correlation with lateral aperture translation: Experimental results and implications for spatial compounding. *IEEE Transactions on Ultrasonics, Ferroelectrics and Frequency Control, 33*(3), 257–264.

Tupholme, G. E. (1969). Generation of acoustic pulses by baffled plane pistons. *Mathematika*, 16 209–224.

Verhoeven, I. T. M., & Thijssen, J. M. (1993). Improvement of lesion detectability by speckle reduction filtering: A quantitative study. *Ultrasonic Imaging, 15*(3), 181–204.

Wang, P., Shen, Y., & Wang, Q. (2007). Gaussian wavelet based dynamic filtering (GWDF) method for medical ultrasound systems. *Ultrasonics, 46*(2), 168–176.

Xiao, D., Ng, W. S., Tsang, C. B., & Abeyratne, U. R. (2007). A region and gradient based active contour model and its application in boundary tracking on anal canal ultrasound images. *Pattern Recognition, 40*(12), 3522–3539.

Xiao, C. Y., Su, Z., & Chen, Y. (2004). A diffusion stick method for speckle suppression in ultrasonic images. *Pattern Recognition Letters, 25*(16), 1867–1877.

Yu, Y., & Acton, S. T. (2002). Speckle reducing anisotropic diffusion. *IEEE Transactions on Medical Imaging, 11*(11), 1260–1270.

Zong, X., Laine, A. F., & Geisse, F. A. (1998). Speckle reduction and contrast enhancement of echocardiograms via multiscale nonlinear processing. *IEEE Transactions on Medical Imaging, 17*(4), 532–540.